



Article

Asymmetric Compensation of Reactive Power Using Thyristor-Controlled Reactors

Martynas Šapurov ^{1,2,*} , Vytautas Bleizgys ^{1,2}, Algirdas Baskys ^{1,2}, Aldas Dervinis ¹,
Edvardas Bielskis ^{1,3} , Sarunas Paulikas ², Nerijus Paulauskas ² and Vytautas Macaitis ²

¹ State Research Institute Center for Physical Sciences and Technology, Sauletekio av. 3, LT-10257 Vilnius, Lithuania; vytautas.bleizgys@ftmc.lt (V.B.); algirdas.baskys@ftmc.lt (A.B.); aldas.dervinis@ftmc.lt (A.D.); edvardas.bielskis@su.lt (E.B.)

² Faculty of Electronics, Vilnius Gediminas Technical University, Naugarduko st. 41, 03227 Vilnius, Lithuania; sarunas.paulikas@vgtu.lt (S.P.); nerijus.paulauskas@vgtu.lt (N.P.); vytautas.macaitis@vgtu.lt (V.M.)

³ Department of Functional Materials and Electronics, Siauliai University, P. Visinskio str. 38, 76352 Siauliai, Lithuania

* Correspondence: martynas.sapurov@ftmc.lt; Tel.: +370-684-70305

Received: 4 May 2020; Accepted: 25 May 2020; Published: 27 May 2020



Abstract: The thyristor-controlled reactor (TCR) compensator for smooth asymmetric compensation of reactive power in a low-voltage utility grid is proposed in this work. Two different topologies of compensator were investigated: topology based on a single-cored three-phase reactor and topology with separate reactors for every phase. The investigation of the proposed TCR compensator was performed experimentally using a developed experimental test bench for 12 kVAr total reactive power. The obtained results show that employment of separate reactors for every phase allows us to control the reactive power in every phase independently, and that the TCR compensator with three single-phase reactors is suitable for smooth and asymmetric compensation of reactive power in a low-voltage utility grid.

Keywords: reactive power; thyristor-controlled reactor; air-gaped reactor; low-voltage utility grid; asymmetric compensation of reactive power; smooth compensation of reactive power

1. Introduction

The number of small grid-connected photovoltaic and wind power plants is constantly growing. These plants supply energy to low-voltage lines of the utility. The quantity of energy supplied by these power plants depends on natural conditions, which often change. On the other hand, the electrical grid loads in low-voltage lines are not just three-phase but single-phase as well, and many of them use reactive power. This leads to the fact that one of the main present-day problems of the electrical grid is compensation of the reactive power in the low-voltage grid [1–18] and since the low-voltage three-phase lines are often loaded asymmetrically [14,19–21], the reactive power, which has to be compensated, is different in different phases.

At present, most parts of reactive power compensation systems in low-voltage lines of the utility are based on the electro-mechanical commutation technology of capacitor banks, which are split into steps connected in parallel to the utility grid [22,23]. However, capacitor banks have fixed discrete reactive power capacity, i.e., the reactive power produced by the capacitor bank cannot be changed smoothly. Therefore, it is impossible to fully compensate reactive power of the utility grid using capacitor banks [24].

Smooth reactive power compensation can be achieved by employing static synchronous compensators (STATCOMs) based on a voltage source inverter [24–30]. STATCOM devices are

capable of compensating for both capacitance and inductance reactive power. The inverter of a STATCOM device produces PWM voltage to the utility grid employing a low pass filter. Capacitance reactive power is supplied if the magnitude of the voltage provided by the inverter is higher than the voltage magnitude of the utility grid. In cases when the magnitude of the inverter voltage is lower than the magnitude of the utility grid voltage, inductive reactive power is consumed. The STATCOM compensator based on inverter has a fast response time and is capable of full reactive power compensation. The main disadvantages are its high price [19,20,31] and that STATCOM devices can provide just symmetric compensation of reactive power in all three phases of the grid [32].

Smooth reactive power compensation can be performed by employing the static VAR compensator (SVC), a shunt-connected variable reactance, which either generates or consumes reactive power. The static VAR compensator is a power electronic device based on thyristor-switched capacitors (TSCs) for discrete control of generated reactive power and thyristor-controlled reactors (TCRs) for smooth control of consumed reactive power [24–27]. A TCR consists of a reactor and a bidirectional thyristor connected in series. Consumed inductive reactive power is controlled by variation of the thyristor firing angle α , where $\alpha = 90$ corresponds to full reactive power and $\alpha = 180$ corresponds to zero reactive power [24–27,33–37]. The first step in this approach is to overcompensate the utility grid using the TSC (to make the utility-grid load slightly capacitive) and after that, by consuming the required amount of inductive reactive power by the TCR, the total compensation of reactive power is achieved.

Despite the fact that research in the field of SVCs has been carried out for many years, the topic is still relevant. This fact is evidenced by many new publications devoted to the theory and application of SVCs, e.g., [4,8,12,38–43]. One of the directions of recent research works in this field is the expansion of SVC application areas [8]. A new area of expansion could be the development and application of the SVC for smooth asymmetric compensation of reactive power in low-voltage grids as a cheaper alternative to the inverter-based STATCOM compensator. The novelty of such work can be proved by the following facts:

1. No one on the market offers the SVC, which is based on TSCs and TCRs, for smooth asymmetric compensation of reactive power in low-voltage grids.
2. There are few publications dedicated to the SVC for smooth compensation of reactive power in low-voltage grids [5–9,44]. However, all these publications are dedicated to symmetric compensation of reactive power in all three phases, and in most of them, just the simulation results are presented.
3. The TCR compensator, which is an essential part of the SVC that allows us to achieve smooth compensation, is developed only for the symmetric compensation of the reactive power and practically is employed just for high and medium voltage lines of the utility grid [4,24–27,35,39,41,45–47].

The novelty of this work is that the proposed TCR compensator is capable of compensating reactive power in a three-phase low-voltage grid utility asymmetrically and that the proper operation of the proposed compensator is proved experimentally, using developed experimental reactors and the test bench of the compensator.

2. The Topology and Operation of the TCR Compensator

The block diagram of the experimental test bench for the investigation of the developed TCR compensator for smooth asymmetric compensation of reactive power for a low-voltage utility grid is presented in Figure 1. It consists of a three-phase power supply ($|U| = 230$ V, $f = 50$ Hz); commutation switches SW1–SW3; zero crossing circuits for each phase; thyristor switches T1–T3 for each phase; control block. The test bench was designed for the experimental investigation of the TCR compensator operation with the three-phase single-cored reactor and with separate reactors for every phase. Therefore, the single-cored three-phase Y-connected reactor (L1) with the middle point connected to neutral, three-phase Y-connected separate phase reactors (L2–L4) with the middle

point connected to neutral and switches SW2 and SW3 for commutation of reactors were included into the structure of the reactive power compensator (Figure 1). The power quality analyzer and oscilloscope were used for the measurement of the reactive and active power and waveforms of utility-grid voltage and current. The investigation was performed in low-voltage lines of the utility for symmetric and asymmetric phase load reactive power compensation. The Δ connection of coils as well as Y-connection with an unconnected midpoint were not used because they are not suitable for asymmetric compensation of the reactive power.

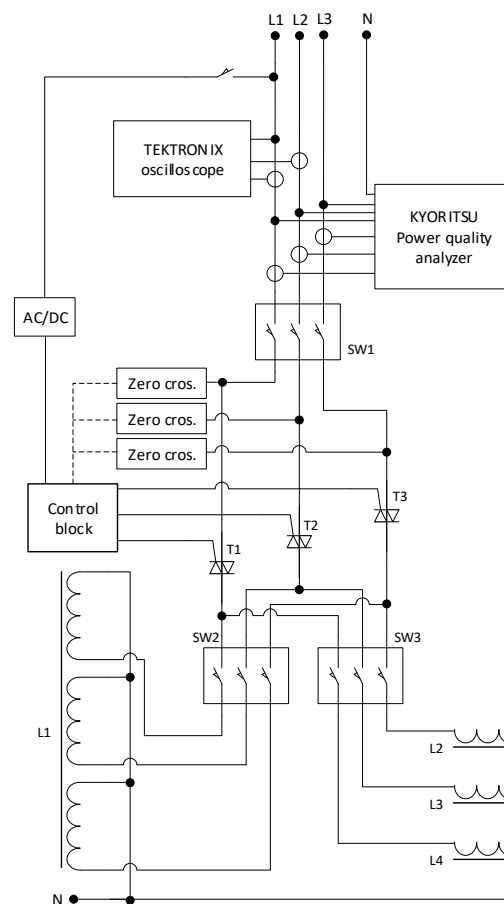


Figure 1. Block diagram of the thyristor-controlled reactor (TCR) compensator experimental test bench.

3. Investigation Results

The experimental investigation results of the proposed TCR compensator for smooth asymmetric compensation of reactive power in a low-voltage utility grid are presented in this section. Two different topologies of compensator are investigated: topology based on a single-cored three-phase reactor and topology with separate reactors for every phase. The main goal of investigations is to prove the possibility of smooth asymmetric compensation of consumed reactive power in a three-phase low-voltage utility grid using a TCR. The experimental test bench of the TCR compensator with a single-cored three-phase reactor is presented in Figure 2.

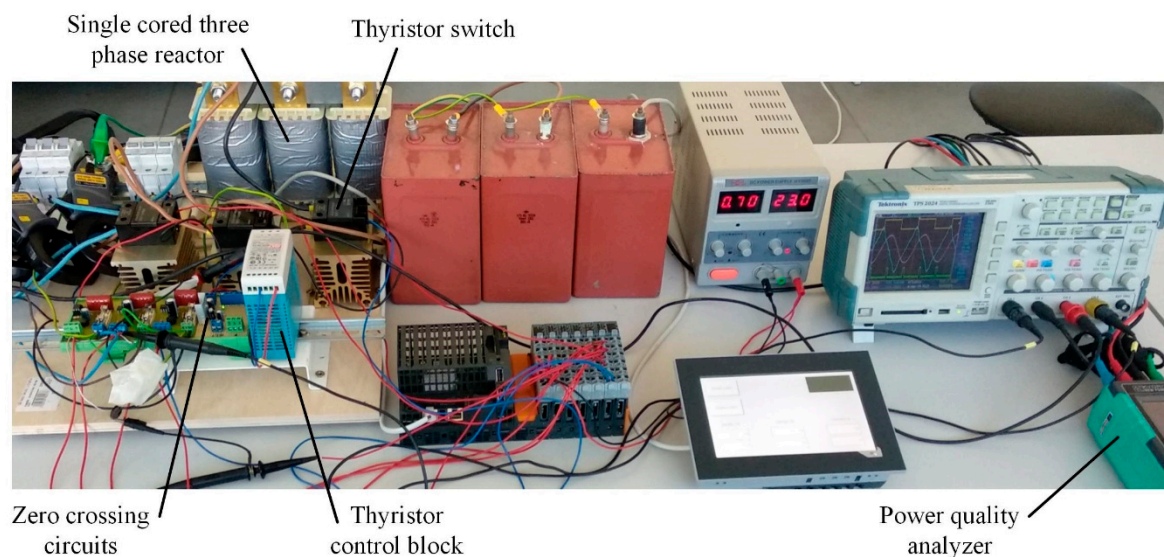


Figure 2. Experimental test bench of the TCR compensator with a single-cored three-phase reactor.

3.1. Investigation of the Compensator Based on a Single-Cored Three-Phase Reactor

The single-cored three-phase air-gaped reactor was designed in order to achieve sufficient reactive power compensation and low consumption of active power and to avoid core saturation. Cores with air gaps are usually used for reactors to avoid their saturation. The theory dedicated to the design of magnetic materials with the air gap, including the cores of reactors, can be found in [48–51]. The three-phase EI-shaped reactor was designed for total reactive power $Q = 4.8$ kVar that corresponds to the RMS of phase current $I = 7$ A for the low-voltage utility-grid phase voltage $|U| = 230$ V. The impedance of the reactor has to be $|Z| = \frac{|U|}{I} \approx 32 \Omega$. The inductive resistance of the coil was much higher than active; therefore, $Z \approx X_L$ and the approximate inductance of the coil can be obtained using the equation $L = \frac{X_L}{\omega} \approx 100$ mH, where ω is the angular frequency of grid voltage. In order to avoid core saturation, the air-gaped core was used. To obtain the desired inductance of the reactor, the approximate design parameters of the reactor coil were chosen using the equation:

$$L = \mu_1 \mu_0 \frac{N^2 \cdot S}{l}, \quad (1)$$

where μ_0 is the free space permeability, μ_1 is the relative magnetic permeability of iron core, N is the number of turns, S is the winding area and l is the length of coil. The parameters of the single-cored three-phase air-gaped reactor are presented in Table 1.

Table 1. Parameters of the single-cored three-phase air-gaped reactor.

Parameter	Value
Relative magnetic permeability of iron core (μ_1)	100
Number of turns of coil (N)	510
Winding area (S)	17.6 cm ²
Length of coil (l)	10.8 cm
Wire cross-section	1.8 mm ²
Inductance of coil at core air gap length $d = 0$	530 mH
Inductance of coil at $d = 6$ mm	100 mH
Inductance of coil at $d = 10$ mm	37 mH
Inductance of coil without core	5.3 mH

By adjusting the air gap, the inductance of every coil was set to 100 mH. The active resistance of every coil is $R = 1 \Omega$. The active resistance in the equivalent circuit of the reactor was connected

in series with the inductive one; therefore, the current was the same for both elements. The values of consumed active power $|P| = 54W$ and reactive power $|Q| = 1.7kVar$ for each phase coil were determined by employing the following equations:

$$|P| = \frac{(|U| \cdot \frac{R}{|Z|})^2}{R}, \quad (2)$$

$$|Q| = \frac{(|U| \cdot \frac{X_L}{|Z|})^2}{X_L}. \quad (3)$$

The structure and view of the designed single-cored air-gaped reactor are presented in Figure 3.

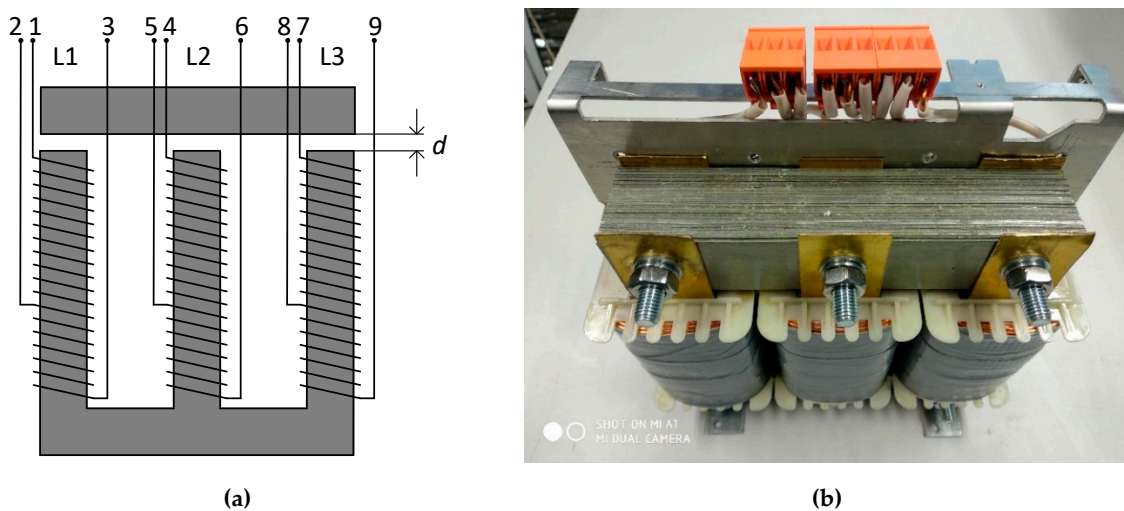


Figure 3. Structure (a) and view (b) of the single-cored three-phase air-gaped reactor.

The reactive power consumed by the reactor is determined by the duration the reactor is connected to the grid. This duration can be controlled by variation of the thyristor firing moment in relation to the grid-voltage zero-value-crossing moment. Usually this moment is named as the thyristor firing angle, α , and is expressed in angular degrees. The obtained reactive power dependences on the firing angle of thyristors, when firing angles in all three phases are changed simultaneously (in the case of symmetric compensation), are presented in Figure 4. The waveforms of utility-grid voltage, reactor current and thyristor firing pulses are given in Figure 5. The obtained results show that the reactive power consumed by the reactor changes in all phases by the same law. The dispersion of the reactive power between individual phases, which is about 17%, is caused by the dispersion of the parameters of the reactor coils. The obtained results allow us to conclude that the TCR compensator based on a single-cored three-phase reactor is suitable for the smooth symmetric compensation of reactive power in all three phases within appropriate error, determined by the dispersion of parameters of reactor coils.

The investigation results prove that the TCR technique can be implemented in a low-voltage utility grid for symmetric compensation of reactive power within appropriate error and that the reactive power consumed by the reactor can be controlled smoothly by control of the thyristor firing angle. Additionally, it can be stated that commutation of the reactor does not introduce any high-frequency disturbances of the reactor current and grid voltage (Figure 5) [52]. However, for the smooth control of the reactive power consumed by the reactor, it was necessary to pass the current only for a certain part of the period. As a result, the reactor current shape was distorted (Figure 5), resulting in low-frequency harmonics.

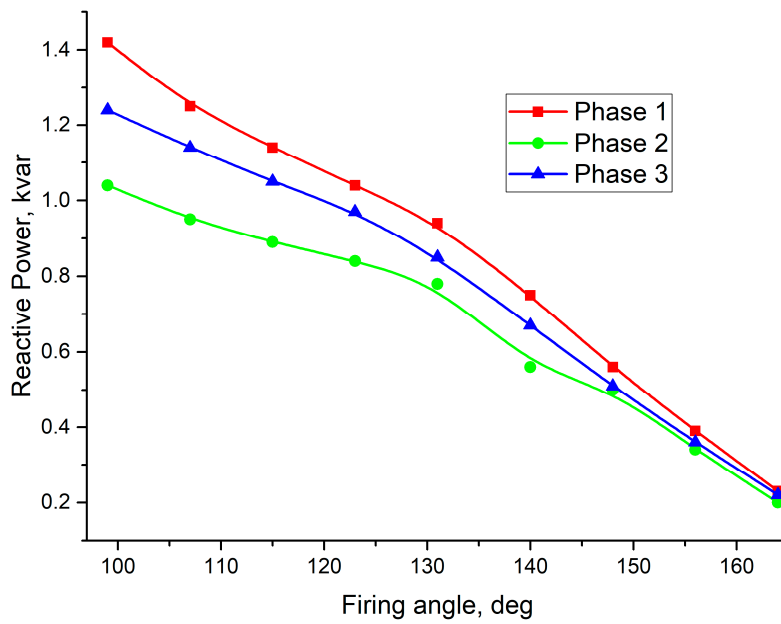


Figure 4. Dependences of reactive power consumed by the single-cored three-phase reactor on the firing angle of the thyristors.

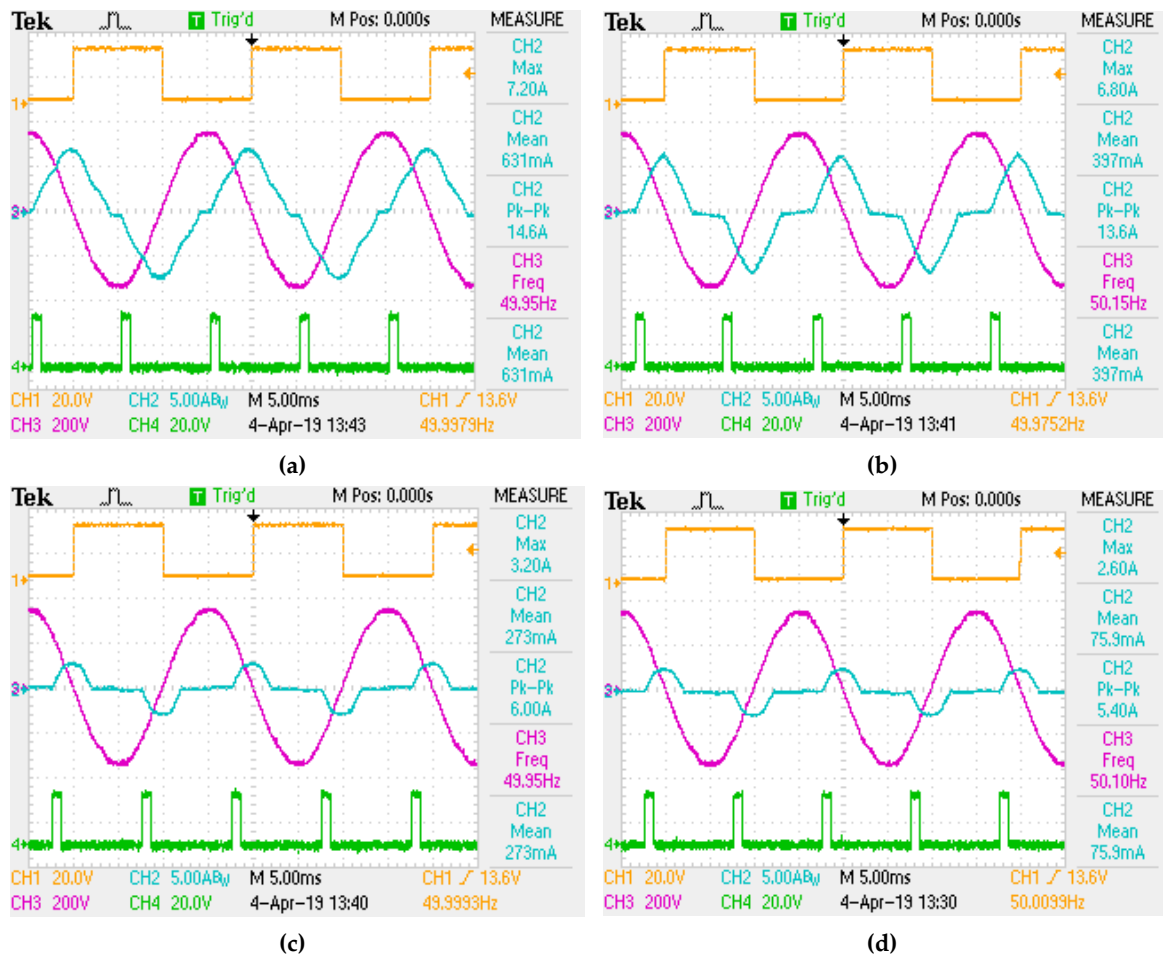


Figure 5. The waveforms of the utility-grid phase voltage (violet) and the reactor current (cyan) on thyristor firing angle (α): (a) 95° (b) 110° (c) 140° and (d) 160°. Voltage zero crossing is displayed in yellow, thyristor control signal in green.

Spectrum analysis was carried out employing an FFT toolbox by importing oscilloscope data into MATLAB/Simulink. The spectrums were obtained experimentally; therefore, harmonic 0 can appear because of measurement error or because the current curve is slightly asymmetric with respect to the time axis, i.e., some DC bias may exist. The asymmetry can be introduced by nonlinearity of our facility network, which can be caused by other devices powered from the same network. The spectrums of reactor current at various thyristor firing angles are presented in Figure 6, and the total harmonic distortion (THD) in Table 2. When a reactor consumes a large amount of reactive energy, which requires the current to flow through the reactor for practically the whole period, the current shape is distorted slightly (Figure 5a). However, for the reduction of the consumed reactive energy, it is necessary for the current to flow through the reactor only for part of the period, so the current shape distortion increases (Figure 5c,d). On the other hand, as the current through the reactor decreases, its effect on the overall distortion of the grid current also decreases.

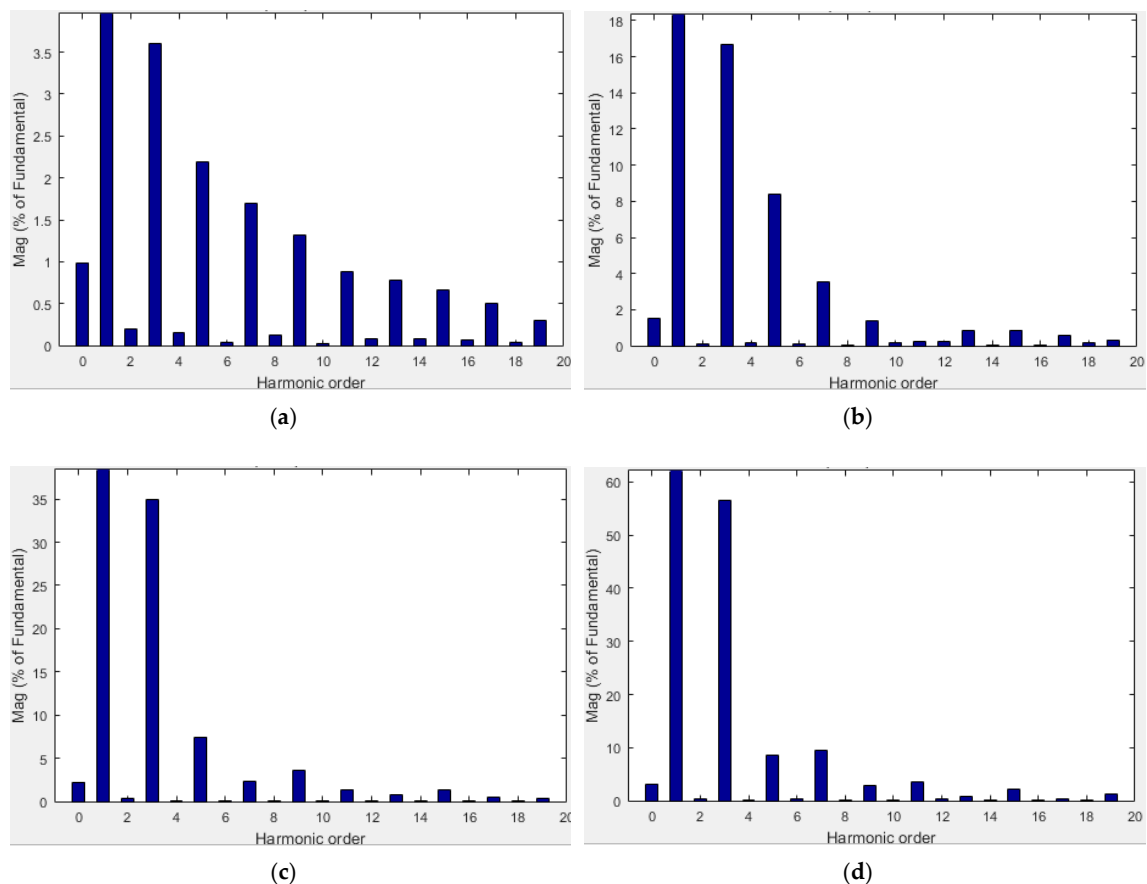


Figure 6. The spectrums of the reactor current at various thyristor firing angles: (a) 95° (b) 110° (c) 140° and (d) 160° . The frequency of the fundamental harmonic is 50 Hz.

Table 2. Total harmonic distortion of the single-cored three-phase air-gaped reactor current.

Thyristor Firing Angle (α)	Total Harmonic Distortion (THD), %
95°	5.2
110°	19.2
140°	36.1
160°	58.3

The next experiment was conducted to determine whether it is possible to control the consumed reactive power in every phase independently, using a single-cored three-phase air-gaped reactor. This is important because only the possibility of independent consumption of reactive power in each phase

allows us to implement asymmetric compensation. The experiment was performed for the case when the firing angles of two phases were fixed: the firing angle of one phase was fixed at 165° (corresponds to minimal reactive power), while the firing angle of another phase at 99° (corresponds to maximal reactive power). The firing angle of the remaining phase was varied. The obtained dependences are presented in Figure 7. It is seen that variation of the firing angle of one phase does not just change the reactive power of the controlled phase but also influences the reactive power of phases with fixed firing angles.

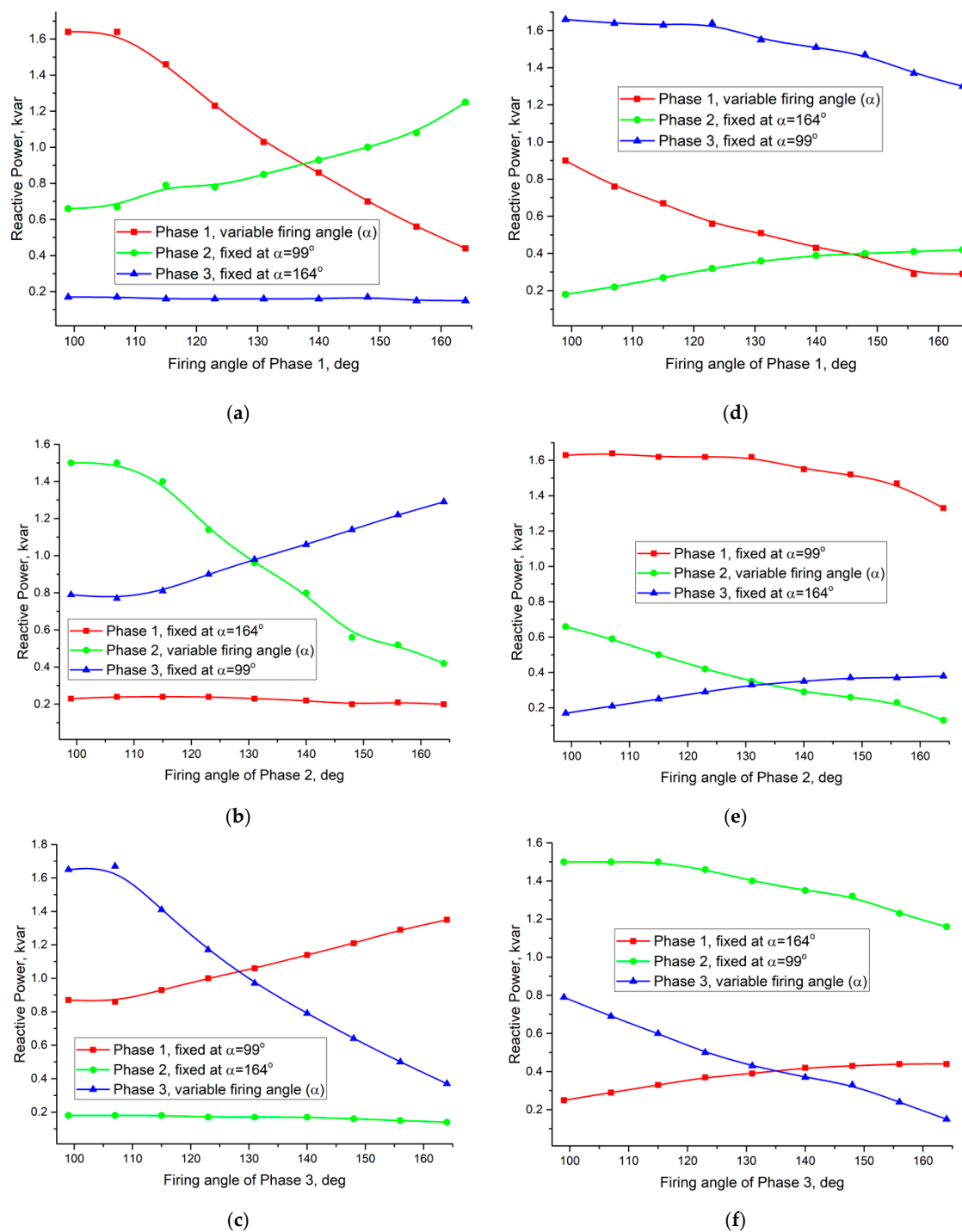


Figure 7. Dependences of reactive power consumed by the single-cored three-phase reactor on the firing angle when the firing angle of one phase is variable and the angles of the remaining two phases are fixed. The Firing angle is variable for Phase 1 (a,d), for Phase 2 (b,e), for Phase 3 (c,f).

The nature of reactive power dependences for the phases with the fixed firing angle depends on the phase sequence. For one sequence, the reactive power was influenced only in one of the phases with a fixed angle (Figure 7a–c). For another sequence, the reactive power of both phases with the fixed firing angles was affected (Figure 7d–f).

During the next experiment, the firing angles of two phases were varied and the angle of the remaining phase was fixed. The investigation was performed for the case when the fixed firing angle was set to $\alpha = 165^\circ$. Dependences of reactive power consumed by the single-cored three-phase reactor on firing angles of two phases are presented in Figure 8. It is seen that reactive power dependences of the phases with the variable firing angle strongly differ in spite of the fact that the firing angles of the thyristors are varied simultaneously. This happens due to one phase being influenced by another through the common core of the reactor.

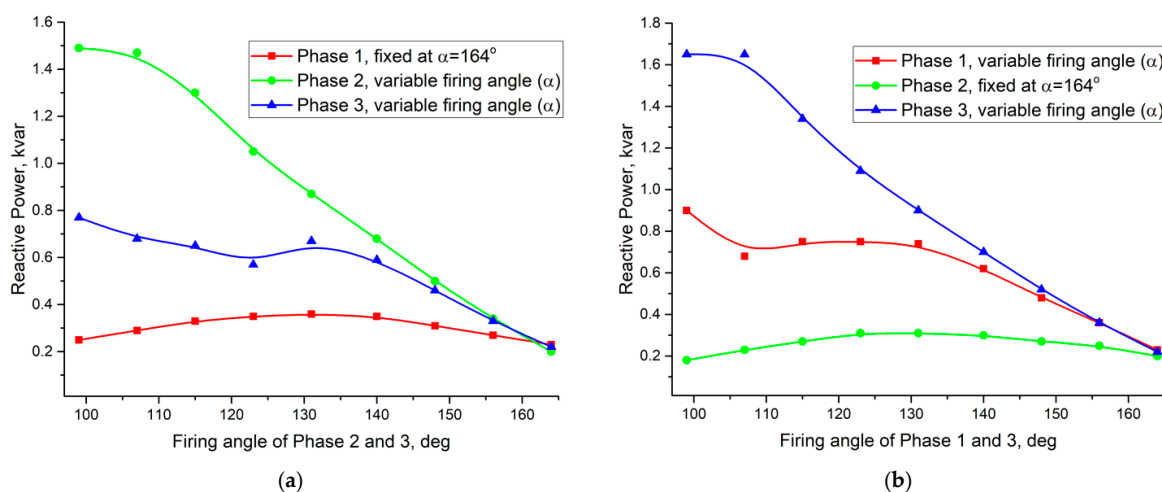


Figure 8. Dependences of reactive power consumed by the single-cored three-phase reactor on the firing angle when the firing angles of the two phases are variable and the angle of the remaining phase is fixed. The Firing angle is variable for Phase 1 (a), for Phase 2 (b).

Summarizing the obtained experimental investigation results, it can be concluded that it is impossible to control the reactive power in every phase independently using a compensator based on a single-cored three-phase reactor. This happens because phases influence each other through the common core of the reactor; therefore, separate reactors must be used for each phase for the asymmetric compensation of reactive power in a low-voltage utility grid.

3.2. Investigation of the Compensator Based on Separate Reactors for Every Phase

The structure and view of the designed air-gaped reactor for single phase are presented in Figure 9. Every single-phase reactor is capable of consuming 4.2 kVAr of reactive power, which corresponds to phase current RMS $I = 18.5$ A for the low-voltage utility-grid phase voltage $|U| = 230$ V. Total reactive power of all three reactors is 12.6 kVAr. The impedance of the reactor is $|Z| = \frac{|U|}{|I|} \approx 12.5 \Omega$; the inductance $L = \frac{X_L}{\omega} \approx 40$ mH. The required 40 mH inductance value was achieved by adjusting the reactor air gap. The parameters of the single-phase air-gaped reactor are presented in Table 3.

The TCR compensator based on three single-phase air-gaped reactors was investigated experimentally. Firstly, the reactive power dependences on the firing angle of thyristors, when firing angles in all three phases were changed simultaneously (in case of case of smooth symmetric compensation), were obtained (Figure 10). It is seen that the reactive power consumed by the single-phase reactors changes in all phases by the same law. The dispersion of the reactive power between individual phases was about 3%. The next experiment was performed in the same way as in the case of the TCR based on a single-cored three-phase air-gaped reactor, i.e., the firing angles of two phases were fixed: The firing angle of one phase was fixed at 165° , while the firing angle of another

phase was fixed at 99° . The firing angle of the remaining phase was varied. The obtained dependences of reactive power consumption of every phase on the firing angle are presented in Figure 11. It is seen that the reactive power consumption of the phase with the variable firing angle has no impact on the reactive power consumption of the remaining two phases with the fixed firing angles. Therefore, this conclusion can be drawn: The employment of three single-phase reactors allows us to control the reactive power in every phase independently, and the compensator with three single-phase reactors is suitable for the smooth asymmetric compensation of reactive power in a low-voltage utility grid.

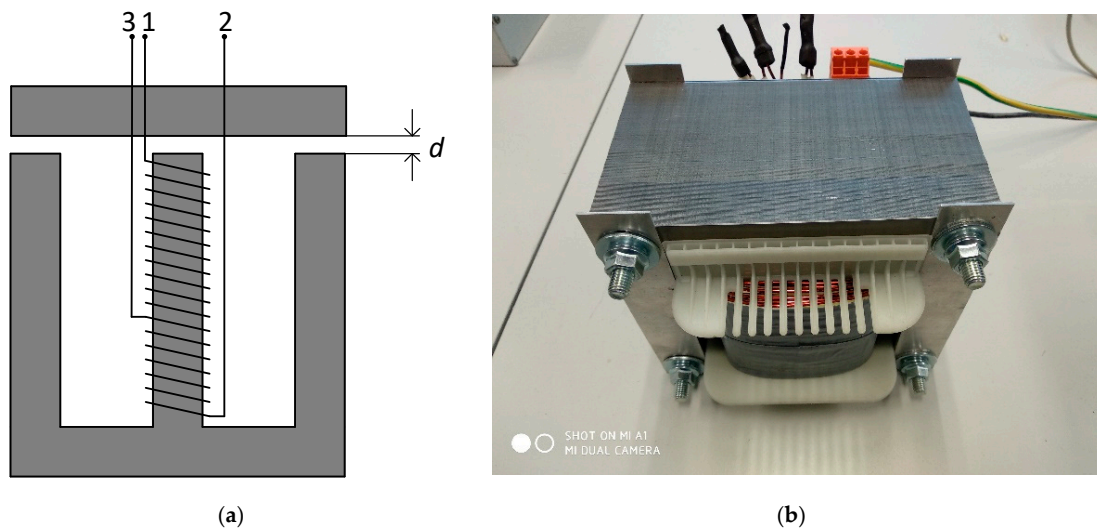


Figure 9. Design (a) and view (b) of the single-phase air-gaped reactor.

Table 3. Parameters of the single-phase air-gaped reactor.

Parameter	Value
Relative magnetic permeability of iron core (μ_1)	100
Number of turns of coil (N)	160
Winding area (S)	71.5 cm ²
Length of coil (l)	9.0 cm
Wire cross-section	3.1 mm ²
Inductance of coil at core air gap length $d = 0$	256 mH
Inductance of coil at $d = 5$ mm	40 mH
Inductance of coil at $d = 10$ mm	18 mH
Inductance of coil without core	2.6 mH

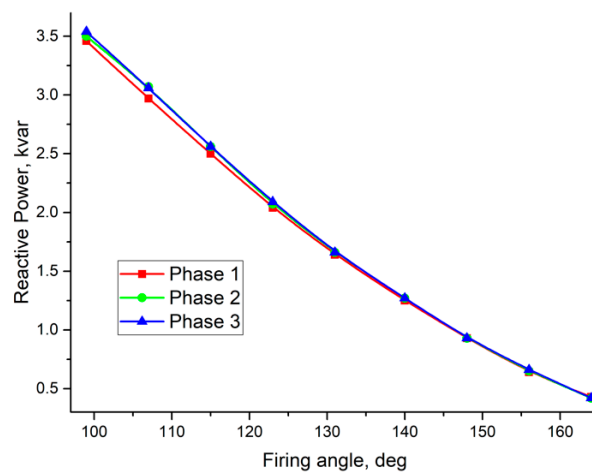


Figure 10. Dependencies of reactive power consumed by the single-phase air-gaped reactors on the firing angle of thyristors.

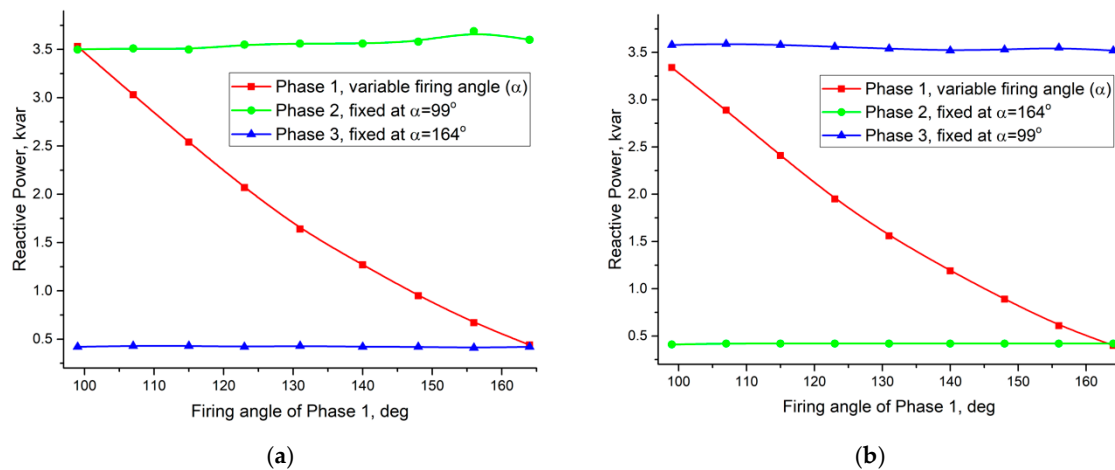


Figure 11. Dependences of reactive power consumed by each single-phase air-gapped reactor on the firing angle when the firing angles of the two phases are fixed and the angle of the remaining phase is variable. The Firing angle is variable for Phase 1 (a), for Phase 2 (b).

It should be mentioned that the investigation also covered the TCR compensator with Δ connection of single-phase reactor coils as well as Y-connection with an unconnected midpoint; however, the investigation results showed that these topologies of the TCR compensator are not suitable for asymmetric load compensation.

3.3. Efficiency of the TCR Compensator

The dependences of reactive and active power of single-cored three-phase and separate-phase air-gapped reactors were measured by applying a symmetric load (Figure 12). The efficiency of reactors was calculated as a ratio of reactive power to total power. Dependences of reactor efficiency on the firing angle are given in Figure 13.

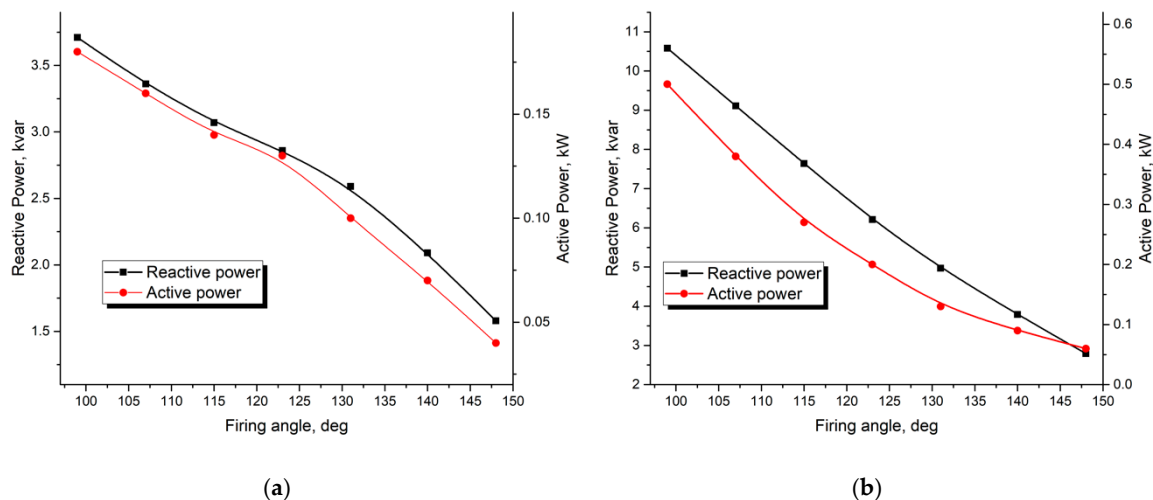


Figure 12. Dependences of reactive and active power consumed by (a) the single-cored three-phase reactor and (b) three single-phase air-gapped reactors.

It could be observed (Figure 13) that the efficiency of the reactors varies from 0.955 to 0.975 when power consumed by the reactors changes from the maximal to minimal value. It is seen that efficiency decreases with increasing of the reactive power (with decreasing of the thyristor firing angle). This appears due to the fact that as the reactive power increases, the reactor current increases, and as a consequence, the active reactor losses increase as well.

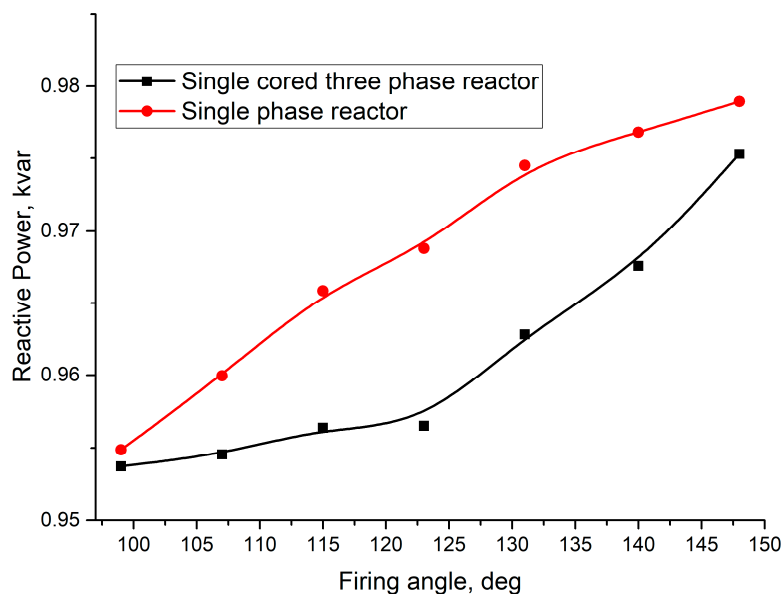


Figure 13. Dependencies of reactor efficiency on the firing angle.

4. Conclusions

1. TCR compensators, which typically are used in high- and medium-voltage utility grids, can be implemented in a low-voltage utility grid employing air-gapped reactors using a Y-connection connected to the neutral midpoint.
2. Variation of the thyristor firing angle of one phase of single-cored three-phase reactor does not just change the reactive power of the controlled phase but influences the reactive power of phases with fixed firing angles. This fact shows that it is impossible to control the reactive power in every phase independently using a TCR compensator based on a single-cored three-phase air-gapped reactor, i.e., a compensator with such a reactor is not suitable for the asymmetric compensation of reactive power.
3. Employment of three single-phase air-gapped reactors allows us to control the reactive power in every phase independently; therefore, a developed TCR compensator based on three single-phase reactors is suitable for smooth and asymmetric compensation of reactive power in a low-voltage utility grid.
4. Commutation of the reactor using thyristor switches does not introduce any high-frequency disturbances of the reactor current and grid voltage.
5. TCR compensator topologies with Δ connection of coils of single-phase reactors as well as Y-connection with unconnected midpoint are not suitable for asymmetric compensation of reactive power in a low-voltage utility grid.
6. The developed single-cored three-phase reactor and single-phase reactors are characterized by 0.955–0.975 efficiency.

Author Contributions: The results presented in this paper were obtained in the framework of a PhD thesis by M.Š., who was supervised by A.B. The experimental measurements performed at the Laboratory of Electronic Systems, Center for Physical Sciences and Technology were supervised by M.Š., V.B., N.P. and A.D. The conceptualization was introduced by S.P., A.B., V.M. and E.B. All authors contributed to the writing of this paper as well as the analysis of the results. All authors have read and agreed to the published version of the manuscript.

Funding: The paper is funded by UAB Lietpak and UAB Navitus under Grant No. 3400-S510.

Acknowledgments: This work was supported, in part, by UAB Lietpak and UAB Navitus under Grant No. 3400-S510.

Conflicts of Interest: The authors declare no conflict of interest.

References

1. Yong, X.; Jiamei, D.; Shuangbao, M. Power flow control of a distributed generation unit in micro-grid. In Proceedings of the 2009 IEEE 6th International Power Electronics and Motion Control Conference, Wuhan, China, 17–20 May 2009; pp. 2122–2125.
2. Trentini, F.; Tasca, M.; Tomasin, S.; Erseghe, T. Reactive power compensation in smart micro grids: A prime-based testbed. In Proceedings of the 2012 IEEE International Energy Conference and Exhibition (ENERGYCON), Florence, Italy, 9–12 September 2012; pp. 909–914.
3. Deblecker, O.; Stevanoni, C.; Vallée, F. Cooperative control of multi-functional inverters for renewable energy integration and power quality compensation in micro-grids. In Proceedings of the 2016 International Symposium on Power Electronics, Electrical Drives, Automation and Motion (SPEEDAM), Anacapri, Italy, 22–24 June 2016; pp. 1051–1058.
4. Ilisiu, D.; Dinu, E.-D. Modern reactive power compensation for smart electrical grids. In Proceedings of the 2019 22nd International Conference on Control Systems and Computer Science (CSCS), Bucharest, Romania, 28–30 May 2019; pp. 353–357.
5. Bogónez-Franco, P.; Balcells, J.; Junyent, O.; Jordà, J. SVC model for voltage control of a microgrid. In Proceedings of the 2011 IEEE International Symposium on Industrial Electronics, Gdansk, Poland, 27–30 June 2011; pp. 1645–1649.
6. Balcells, J.; Bogónez-Franco, P. Voltage control in a LV microgrid by means of an SVC. In Proceedings of the IECON 2013-39th Annual Conference of the IEEE Industrial Electronics Society, Vienna, Austria, 10–13 November 2013; pp. 6027–6030.
7. Beck, Y.; Berkovich, Y.; Müller, Z.; Tlustý, J. A Matlab-Simulink model of network reactive power compensation based on binary switchable capacitors and thyristor-controlled reactor. In Proceedings of the 2016 IEEE International Conference on the Science of Electrical Engineering (ICSEE), Eilat, Israel, 16–18 November 2016; pp. 1–5.
8. Beck, Y.; Berlovich, Y.; Braunstein, A. A Matlab-Simulink model of AC grid with a FC-TCR and invariant control system for reactive power compensation. In Proceedings of the 2016 International Symposium on Power Electronics, Electrical Drives, Automation and Motion (SPEEDAM), Anacapri, Italy, 22–24 June 2016; pp. 1292–1297.
9. Dong, T.; Li, L.; Ma, Z. A combined system of APF and SVC for power quality improvement in microgrid. In Proceedings of the 2012 Power Engineering and Automation Conference, Wuhan, China, 18–20 September 2012; pp. 1–4.
10. Ali, Z.; Christofides, N.; Hadjidemetriou, L.; Kyriakides, E. Photovoltaic reactive power compensation scheme: An investigation for the Cyprus distribution grid. In Proceedings of the 2018 IEEE International Energy Conference (ENERGYCON), Limassol, Cyprus, 3–7 June 2018; pp. 1–6.
11. Arshad, A.; Lehtonen, M. Instantaneous active/reactive power control strategy for flicker mitigation under high PV penetration. In Proceedings of the 2018 IEEE PES Innovative Smart Grid Technologies Conference Europe (ISGT-Europe), Sarajevo, Bosnia and Herzegovina, 21–25 October 2018; pp. 1–6.
12. Stanelyte, D.; Radziukynas, V. Review of voltage and reactive power control algorithms in electrical distribution networks. *Energies* **2020**, *13*, 58. [[CrossRef](#)]
13. Gayatri, M.T.L.; Parimi, A.M.; Kumar, A.V.P. A review of reactive power compensation techniques in microgrids. *Renew. Sustain. Energy Rev.* **2018**, *81*, 1030–1036. [[CrossRef](#)]
14. Charalambous, A.; Hadjidemetriou, L.; Zacharia, L.; Bintoudi, A.D.; Tsolakis, A.C.; Tzovaras, D.; Kyriakides, E. Phase balancing and reactive power support services for microgrids. *Appl. Sci.* **2019**, *9*, 5067. [[CrossRef](#)]
15. Li, B.; Tian, X.; Zeng, H. A grid-connection control scheme of PV system with fluctuant reactive load. In Proceedings of the 2011 4th International Conference on Electric Utility Deregulation and Restructuring and Power Technologies (DRPT), Weihai, China, 6–9 July 2011; pp. 786–790.
16. Santacana, E.; Rackliffe, G.; Tang, L.; Feng, X. Getting Smart. *IEEE Power Energy Mag.* **2010**, *8*, 41–48. [[CrossRef](#)]
17. Bielskis, E.; Baskys, A.; Valiulis, G. Controller for the grid-connected microinverter output current tracking. *Symmetry* **2020**, *12*, 112. [[CrossRef](#)]
18. Bielskis, E.; Baskys, A.; Sapurov, M. Single stage microinverter based on two-switch DC-DC flyback converter. *Elektron. Ir Elektrotechnika* **2017**, *23*, 29–32. [[CrossRef](#)]

19. Pană, A.; Băloi, A.; Molnar-Matei, F. From the balancing reactive compensator to the balancing capacitive compensator. *Energies* **2018**, *11*, 1979. [CrossRef]
20. Pană, A.; Băloi, A.; Molnar-Matei, F. Iterative method for determining the values of the susceptances of a balancing capacitive compensator. *Energies* **2018**, *11*, 2742. [CrossRef]
21. Xiang-Qian, T.; Keqing, X.; Ming, S.; Xianhong, M. Reactive power and unbalance compensation with DSTATCOM. In Proceedings of the 2005 International Conference on Electrical Machines and Systems, Nanjing, China, 27–29 September 2005; Volume 2, pp. 1181–1184.
22. Fuchs, E.; Masoum, M.A.S. *Power Quality in Power Systems and Electrical Machines*; Academic Press: Cambridge, MA, USA, 2011; ISBN 978-0-08-055917-9.
23. Igbinoia, F.; Fandi, G.; Svec, J.; Muller, Z.; Tlustý, J. Comparative review of reactive power compensation technologies. In Proceedings of the 2015 16th International Scientific Conference on Electric Power Engineering, Ostrava, Czech Republic, 20–22 May 2015; pp. 2–7. [CrossRef]
24. Acha, E.; Agelidis, V.; Anaya-Lara, O.; Miller, T.J.E. *Power Electronic Control in Electrical Systems*; Newnes: Oxford, UK, 2002; ISBN 978-0-7506-5126-4.
25. Dixon, J.; Moran, L.; Rodriguez, J.; Domke, R. Reactive power compensation technologies: State-of-the-art review. *Proc. IEEE* **2005**, *93*, 2144–2164. [CrossRef]
26. Padiyar, R.K. *Facts Controllers in Power Transmission and Distribution*; New Age International (P) Ltd.: New Delhi, India, 2007; ISBN 978-81-224-2541-3.
27. Mathur, R.M.; Varma, R.K. *Thyristor-Based FACTS Controllers for Electrical Transmission Systems*; John Wiley & Sons: Hoboken, NJ, USA, 2002; ISBN 978-0-470-54668-0.
28. Tehrani, K.-A.; Capitaine, T.; Barrandon, L.; Hamzaoui, M.; Rafiei, S.M.R.; Lebrun, A. Current control design with a fractional-order PID for a three-level inverter. In Proceedings of the Proceedings of the 2011 14th European Conference on Power Electronics and Applications, Birmingham, UK, 30 August–1 September 2011; pp. 1–7.
29. Xu, Y.; Tolbert, L.M.; Kueck, J.D.; Rizy, D.T. Voltage and current unbalance compensation using a static var compensator. *IET Power Electron.* **2010**, *3*, 977–988. [CrossRef]
30. Chang, W.-N.; Liao, C.-H. Design and implementation of a STATCOM based on a multilevel FHB converter with delta-connected configuration for unbalanced load compensation. *Energies* **2017**, *10*, 921. [CrossRef]
31. PQC-Statcon. Available online: https://library.e.abb.com/public/2b588b8dd20ce996c1257a37003639e4/PQC-STATCON_Flyer.pdf (accessed on 6 November 2019).
32. Yan, J. *Handbook of Clean Energy Systems*, 1st ed.; John Wiley & Sons: Chichester, UK, 2015; Volume 6, ISBN 978-1-118-38858-7.
33. Panfilov, D.I.; ElGebaly, A.E. Modified thyristor controlled reactor for static VAR compensators. In Proceedings of the 2016 IEEE International Conference on Power and Energy (PECon), Melaka, Malaysia, 28–29 November 2016; pp. 712–717.
34. Khonde, R.S.; Palandurkar, M.V. Simulation model of thyristor controlled reactor. *Int. J. Eng. Res. Technol.* **2014**, *3*, 1692–1694.
35. Panfilov, D.I.; ElGebaly, A.E.; Astashev, M.G. Design and evaluation of control system for static VAR compensators with thyristors switched reactors. In Proceedings of the 2017 IEEE 58th International Scientific Conference on Power and Electrical Engineering of Riga Technical University (RTUCON), Riga, Latvia, 12–13 October 2017; pp. 1–6.
36. Mahapatra, S.; Goyal, A.; Kapil, N. Thyristor controlled reactor for power factor improvement. *Int. J. Eng. Res. Appl.* **2014**, *4*, 55–59.
37. Awad, F.; Mansour, A.; Elzhab, E. Thyristor controlled reactor with different topologies based on fuzzy logic controller. *Int. J. Eng. Res.* **2015**, *4*, 498–505. [CrossRef]
38. Panfilov, D.I.; ElGebaly, A.E.; Astashev, M.G. Topologies of thyristor controlled reactor with reduced current harmonic content for static VAR compensators. In Proceedings of the 2017 IEEE International Conference on Environment and Electrical Engineering and 2017 IEEE Industrial and Commercial Power Systems Europe (EEEIC / I CPS Europe), Milan, Italy, 6–9 June 2017; pp. 1–6.
39. Čerňan, M.; Tlustý, J. Study of the susceptance control of industrial static var compensator. In Proceedings of the 2015 16th International Scientific Conference on Electric Power Engineering (EPE), Kouty nad Desnou, Czech Republic, 20–22 May 2015; pp. 538–541.

40. Hong, H.; Wenmei, W.; Shaohua, X.; Min, T.; Chuanjia, H. Summary on reactive power compensation technology and application. In Proceedings of the 2nd International Conference on Intelligent Computing and Cognitive Informatics (ICICCI 2015), Singapore, 8–9 September 2015.
41. Farkoush, S.G.; Kim, C.-H.; Rhee, S.-B. THD reduction of distribution system based on ASRFC and HVC method for SVC under EV charger condition for power factor improvement. *Symmetry* **2016**, *8*, 156. [[CrossRef](#)]
42. Alkayyali, M.; Ghaeb, J. Hybrid PSO–ANN algorithm to control TCR for voltage balancing. *IET Gener. Transm. Distrib.* **2020**, *14*, 863–872. [[CrossRef](#)]
43. Panfilov, D.I.; Rozhkov, A.N.; Astashev, M.G.; Zhuravlev, I.I. Modern approaches to controlled static VAR compensators design. In Proceedings of the 2019 IEEE International Conference on Environment and Electrical Engineering and 2019 IEEE Industrial and Commercial Power Systems Europe (EEEIC/I CPS Europe), Genova, Italy, 11–14 June 2019; pp. 1–5.
44. Köse, A.; Irmak, E. Modeling and simulation of a static VAR compensator based on FC-TCR. In Proceedings of the 2016 IEEE International Conference on Renewable Energy Research and Applications (ICRERA), Birmingham, UK, 20–23 November 2016; pp. 924–927.
45. Rahmani, S.; Hamadi, A.; Al-Haddad, K.; Dessaint, L.A. A Combination of shunt hybrid power filter and thyristor-controlled reactor for power quality. *IEEE Trans. Ind. Electron.* **2014**, *61*, 2152–2164. [[CrossRef](#)]
46. Liberado, E.V.; Souza, W.A.; Pomilio, J.A.; Paredes, H.K.M.; Marafão, F.P. Design of static VAR compensator using a general reactive energy definition. In Proceedings of the International School on Nonsinusoidal Currents and Compensation 2013 (ISNCC 2013), Zielona Góra, Poland, 20–21 June 2013; pp. 1–6.
47. Tokiwa, A.; Yamada, H.; Tanaka, T.; Watanabe, M.; Shirai, M.; Teranishi, Y. New hybrid static VAR compensator with series active filter. *Energies* **2017**, *10*, 1617. [[CrossRef](#)]
48. Arab-Tehrani, K.; Colteu, A.; Rasoanarivo, I.; Michel-Sargos, F. Design a new high intensity magnetic separator with permanent magnets for industrial applications. *Int. J. Appl. Electromagn. Mech.* **2010**, *32*, 237–248. [[CrossRef](#)]
49. Topaloglu, I. Air gap optimization of iron core shunt reactors with discretely disturbed air gaps for UHV systems. In Proceedings of the International conference on engineering and natural science (ICENS 2016), Sarajevo, Bosnia and Herzegovina, 24–28 May 2016; pp. 1–6.
50. Wass, T.; Hörnfeldt, S.; Valdemarsson, S. The design and construction of a controllable reactor with a HTS control winding. *J. Phys. Conf. Ser.* **2006**, *43*, 873. [[CrossRef](#)]
51. Bielskis, E.; Baskys, A.; Sapurov, M. Impact of transformer design on flyback converter voltage spikes. *Elektron. Ir Elektrotechnika* **2016**, *22*, 58–61. [[CrossRef](#)]
52. Šapurov, M.; Bielskis, E.; Bleizgys, V.; Dervinis, A. Stepless compensator of reactive power. *Moksl. Liet. Ateitis Sci. Future Lith.* **2020**, *12*. [[CrossRef](#)]



© 2020 by the authors. Licensee MDPI, Basel, Switzerland. This article is an open access article distributed under the terms and conditions of the Creative Commons Attribution (CC BY) license (<http://creativecommons.org/licenses/by/4.0/>).